2023

Formation of undulating seafloor bedforms during the Minoan eruption and their implications for eruption dynamics and slope stability at Santorini

Jens Karstens

Jonas Preine

Steven Carey
University of Rhode Island, scarey@uri.edu

Katherine L.C. Bell

Paraskevi Nomikou

See next page for additional authors

Citation/Publisher Attribution

Karstens, J., Preine, J., Carey, S., Bell, K. L.C., Nomikou, P., Hübscher, C.,...Urlaub, M. (2023). Formation of undulating seafloor bedforms during the Minoan eruption and their implications for eruption dynamics and slope stability at Santorini. *Earth and Planetary Science Letters, 616*, 118215. https://doi.org/10.1016/j.epsl.2023.118215
Available at: https://doi.org/10.1016/j.epsl.2023.118215

Formation of undulating seafloor bedforms during the Minoan eruption and their implications for eruption dynamics and slope stability at Santorini

Authors

Jens Karstens, Jonas Preine, Steven Carey, Katherine L.C. Bell, Paraskevi Nomikou, Christian Hübscher, Danai Lampridou, and Morelia Urlaub

Creative Commons License

This work is licensed under a Creative Commons Attribution 4.0 License.

Earth and Planetary Science Letters 616 (2023) 118215

Contents lists available at ScienceDirect

Earth and Planetary Science Letters

journal homepage: www.elsevier.com/locate/epsl

Formation of undulating seafloor bedforms during the Minoan eruption and their implications for eruption dynamics and slope stability at Santorini

Jens Karstens [a,*], Jonas Preine [b], Steven Carey [c], Katherine L.C. Bell [d], Paraskevi Nomikou [e], Christian Hübscher [b], Danai Lampridou [e], Morelia Urlaub [a]

[a] GEOMAR Helmholtz-Zentrum für Ozeanforschung Kiel, Germany
[b] University of Hamburg, Institute of Geophysics, Hamburg, Germany
[c] University of Rhode Island, Kingston, USA
[d] Ocean Discovery League, Saunderstown, RI, USA
[e] National and Kapodistrian University of Athens, Athens, Greece

ARTICLE INFO

Article history:
Received 1 December 2022
Received in revised form 4 May 2023
Accepted 7 May 2023
Available online 7 June 2023
Editor: C.M. Petrone

Dataset link: https://doi.pangaea.de/10.1594/PANGAEA.956579

Keywords:
undulating seafloor bedform
slope instability
pyroclastic flows
Minoan eruption
Santorini

ABSTRACT

The Minoan eruption of Santorini is one of the largest Holocene volcanic events and produced several cubic kilometers of pyroclastic flows emplaced on the submerged flanks of the volcano. Marine geophysical surveys reveal a multitude of undulating seafloor bedforms (USBs) around Santorini. While similar structures are known from other volcanoes worldwide, Santorini offers the unique opportunity to relate USB formation with volcanic processes during one of the best-studied volcanic eruptions worldwide. In this study, we combine high-resolution seismic reflection data with multibeam echosounder bathymetry to reveal the internal architecture of USBs around Santorini and to relate their morphological characteristics to formational processes. The USBs around Santorini were formed during the Minoan eruption and represent the seafloor expression of mass transport deposits. Three types of deposits differ in composition or origin. (1) Depositional USBs, which can only be found to the north of the island, where Minoan eruption ignimbrites reach their maximum thickness and the undulating topography is the result of thrusting within the deposit. (2) USBs related to slope failures of volcaniclastics from the entire Thera Pyroclastic Formation, which can be found east, south, and west of the island. (3) USBs associated with deep-seated deformation, which occurs on the southwestern flank along an area affected by rift tectonics and extends to a depth of more than 200 m below the seafloor. In cases (2) and (3), the USBs are formed upslope by block rotation and downslope by thrusting. Our study indicates that these processes may have contributed to the generation of the devastating Minoan tsunami. Since Santorini is located in one of the most tectonically active regions in the Mediterranean, capable of producing earthquakes with magnitude M7+, our study has important implications for hazard assessment. A strong earthquake located close to the island may have the potential to reactivate slope instabilities posing a previously undetected but potentially significant tsunami hazard.

1. Introduction

The Minoan eruption of Santorini in the Aegean Sea is considered one of the largest explosive volcanic eruptions in the Holocene (Sigurdsson et al., 2006; Johnston et al., 2014). Santorini lies in the center of the Hellenic Arc (**Fig. 1**) and has experienced at least four caldera-forming eruptions, with the 1600 BCE Minoan eruption being the latest and largest (Druitt et al., 1999; Satow et al., 2021). Within hours to days, Santorini discharged vast amounts of gas-charged magma, sending tephra, pyroclastic flows, aerosols, and tsunamis across the eastern Mediterranean (Druitt et al., 2019a). During the eruption, large parts of the island collapsed, leaving behind a flooded caldera, which dominates Santorini's present-day landscape. The eruption had disastrous consequences for the people that populated the islands of the Aegean Sea in the Late Bronze Age and possibly contributed to the decline of the great Minoan civilization (Druitt et al., 2019b). Deposits of the Minoan eruption cover the seafloor around Santorini (Sigurds-

* Corresponding author.
E-mail address: jkarstens@geomar.de (J. Karstens).

https://doi.org/10.1016/j.epsl.2023.118215

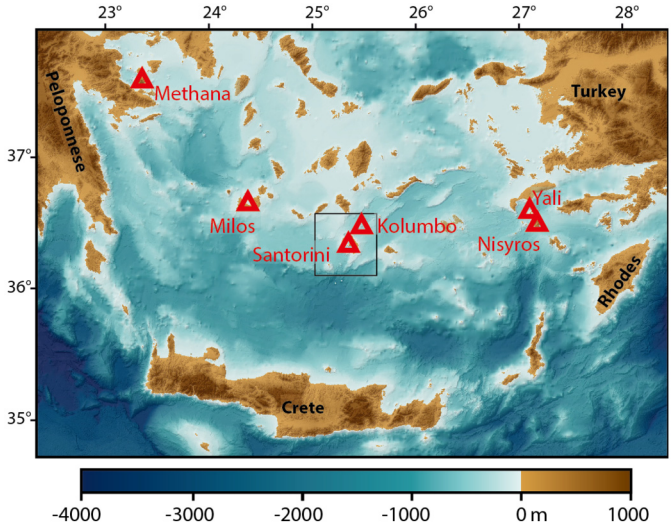

Fig. 1. Map of the Aegean Sea showing the location of volcanic centers of the Hellenic Arc and the study area (box). Elevation is relative to sea level. Data source: EMODnet Bathymetry Consortium (2020).

son et al., 2006; Karstens et al., 2023), which is characterized by a multitude of undulating seafloor bedforms (USBs) extending up to 25 km from the volcano (Bell, 2011; Hooft et al., 2017). Such undulating bedforms have been identified in a variety of geological settings, ranging from deep-sea fans to continental shelves, and can result from seabed modification by density flows, internal waves, and mass movement (e.g., Lee et al., 2002; Cartigny et al., 2011; Reiche et al., 2018). Extensive fields of USBs have been recognized on the submarine flanks of large-caldera forming volcanic centers, which comprise some of the largest amplitudes ever documented on the seafloor (e.g., Symons et al., 2016). Two recent studies by Pope et al. (2018) and Casalbore et al. (2021) identified two different processes for the formation of USBs at volcanic islands: (1) the deposition of eruption-fed density flows and (2) deformation by slope failure. However, deciphering the different formational processes can be challenging and requires a combination of high-resolution multibeam bathymetry and, most importantly, seismic profiles obtained across the trend of the wave fields (Casalbore et al., 2021).

Santorini has been affected by both major caldera-forming eruptions (Druitt et al., 2019a) and large-scale mass-wasting events (Bell et al., 2013; Nomikou et al., 2016; Preine et al., 2022b). However, the influence of both processes on the formation of USBs at Santorini has not been resolved. In this study, we use an extensive collection of high-resolution multi-channel seismic data collected onboard R/V *Poseidon* (Karstens et al., 2019) and high-resolution bathymetric data to reconstruct the nature and origin of the USBs, as well as the implications for hazard assessment around Santorini. Our first objective is to characterize the morphology of the USBs and compare them with bedforms around other volcanic islands. Our second objective is to identify and reconstruct the processes controlling the formation of USBs around Santorini, including the relevance of pyroclastic flow deposition and slope instabilities in the formation of USBs. Finally, our third objective is to discuss the implications of USB formation on slope stability and geohazard assessment for Santorini.

2. Geological background

The Hellenic Arc consists of the Methana peninsula, the islands of Poros, Milos, Santorini, Kos, and Nisyros, as well as the submarine volcanoes of the Kolumbo volcanic chain (**Fig. 1**) and has been active from the Late Pliocene to the Holocene (Sigurdsson et al., 2006; Nomikou et al., 2012). The Santorini caldera in the center of the arc is the most prominent manifestation of the Christiana-Santorini-Kolumbo volcanic field, hosting some of the largest explosive eruptions in the Mediterranean region. The CSK field has been active since the early Pliocene, with periodic cycles of volcanism and dormancy (Preine et al., 2022a). During the most recent volcanic phase of Santorini since ~0.36 Ma, there have been twelve major and numerous minor eruptions, as well as at least four caldera collapses creating the Thera Pyroclastic Formation (TPF) (Druitt et al., 1999, 2019a). The last major explosive eruption, known as the Late Bronze Age (LBA) or Minoan eruption, occurred approximately 3600 years before present (Bond and Sparks, 1977; Friedrich et al., 2006; Druitt et al., 2019b) and represents the largest and most prominent event in Santorini's history (Satow et al., 2021). Volume estimates for the Minoan eruption vary significantly between 19 and 86 km^3 dense-rock equivalent (DRE; Heiken and McCoy, 1984; Johnston et al., 2014), while the latest reconstruction integrating geophysical and sedimentological constraints indicates a volume of 34.5 ± 6.8 km^3 DRE (Karstens et al., 2023) making it one of the largest in the Holocene. The Minoan eruption occurred in a terrestrial to shallow marine setting of a preexisting caldera connected to the sea. It began with explosive eruptions from onshore vents on a pre-Kameni island in the caldera's center (Druitt et al., 1999; 2019b; Johnston et al., 2014). After several hours, the eruption migrated into the flooded part of the caldera, where the interaction with seawater caused violent phreatomagmatic explosions and the subsequent formation of a tuff cone that filled up the pre-existing caldera and blocked the connection to the sea (Druitt et al., 1999; 2019b; Johnston et al., 2014). After all water in the caldera was displaced, several cubic kilometers of pyroclastic flows entered the sea, causing destructive tsunamis. The subsequent caldera collapse formed the archipelago's present-day topography (Druitt et al., 1999; 2019b; Johnston et al., 2014). Volcanism reemerged with the buildup of Palea and Nea Kameni islands in the caldera's center with the latest eruption in 1950 (Nomikou et al., 2014).

3. Data and methods

This study uses high-resolution multi-channel seismic profiles collected during research cruise POS538 on board R/V *Poseidon* in October 2019 (Karstens et al., 2020). As the seismic source, we used a GI-airgun in harmonic mode with a primary (Generator) and a secondary (Injector) volume of 45 in^3. Seismic signals were recorded by a Geometrics GeoEel streamer with active streamer lengths between 190 m to 250 m. The processing flow included surface-related multiple elimination and pre-stack time migration. The data have a horizontal resolution of ~1.56 m and a vertical resolution of 4-8 m at the seafloor (assuming a seismic velocity of 1,600 m/s). These datasets were analyzed using the seismic interpretation software suites Kingdom Suite by IHS and Petrel by Schlumberger.

The analyzed digital elevation model is a merge (Fig. 2) of satellite-derived Advanced Spaceborne Thermal Emission and Reflection Radiometer (ASTER), Community-sourced DEM from European Marine Observation and Data Network (EMODnet), data acquired on board R/V Aegaeo (Nomikou et al., 2012) during GEOWARN project and R/V Marcus G. Langseth during the PROTEUS project (Hooft et al., 2017; Huff et al., 2021). The swath dataset has a lateral resolution of 20 m and was collected with SEABEAM 2120 20 kHz swath system on R/V Aegaeo and Simrad Kongsberg EM122 12 kHz multibeam echo sounder on R/V Marcus Langseth and processed using the MB-SYSTEM software suite (see Nomikou et al., 2012; Hooft et al., 2017 for details). In addition, we use bathymetric data collected with an autonomous underwater vehicle (AUV) during cruise POS510 (Hannington, 2018) through seven

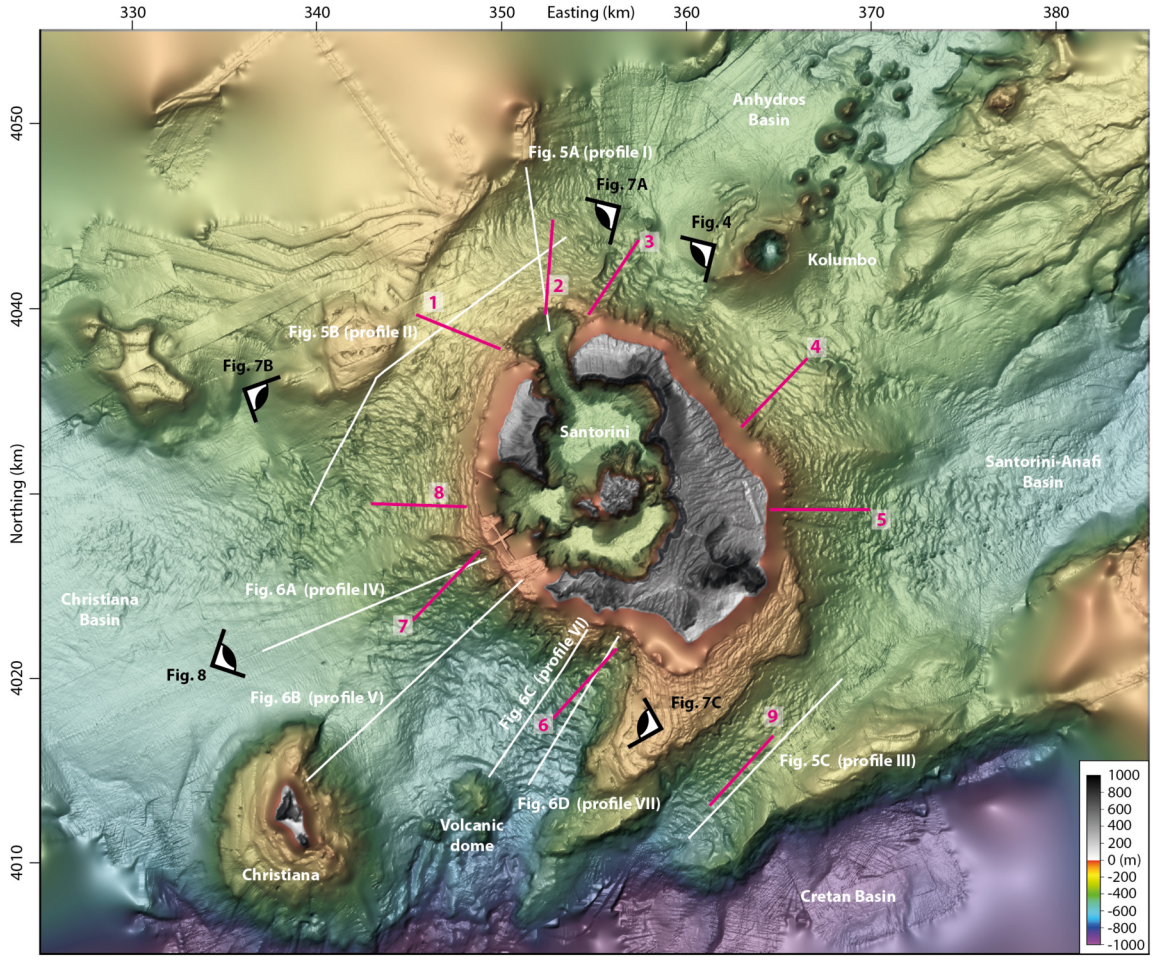

Fig. 2. Shaded bathymetric map of the study area with white lines indicating the location of high-resolution seismic reflection profiles (Roman numbers) and morphologic profiles (pink lines, Arabic numbers) presented in Fig. 3.

dives by AUV Abyss that was equipped with the dual frequency (200/400 kHz) RESON Seabat 7125 multibeam. The data were processed using the MB-SYSTEM software suite and have a lateral resolution of 2 m. To combine seismic and bathymetric data, we applied a seismic velocity of 1,500 m/s for the depth-time conversion.

We extracted nine elevation profiles (**Fig. 3** and **Supplement S1**) to constrain the wavelength and amplitude of the undulating seafloor bedforms and compared them with morphometric results from other volcanoes. We calculated regression curves along each profile and subtracted these from the original profiles to highlight undulations and to better constrain mean wave heights (measured from trough to peak) and wavelengths (measured from peak to peak). Finally, we compare the extracted values for Santorini with wave height, and wavelength values from other volcanoes on a logarithmic plot (**Fig. 3D**) based on Pope et al. (2018) and Casalbore et al. (2021).

4. Results

4.1. Seafloor morphology around Santorini

USBs occur on all sides of Santorini and are particularly pronounced on the eastern, western, and southwestern flanks (**Fig. 2**). They formed on slopes with mean angles of 3.3°, are present in depths of approx. 100 to 700 m below sea level, and extend up to 25 km from the caldera rim. Figure 3 shows three representative bathymetric profiles crossing the northern (A), southwestern (B), and western (C) slopes of Santorini and a logarithmic plot comparing USB wavelengths and wave heights from Santorini derived from nine bathymetric profiles (A-C and supplement S1) with USBs of other volcanoes (D). The USBs around Santorini have heights ranging from 1 to 60 m and wavelengths between 150 and 1,200 m and most of the undulations are asymmetrical (**Fig. 3**). In the logarithmic plot, the USBs arrange linearly and lie in the region of large-scale bedforms (profiles 3, 4, 7, 8, 9) and the intermediate area between large- and small-scale bedforms (profiles 1, 2, 5) (Symons et al., 2016). The smallest wavelengths (130-550 m) and wave heights (1-9 m) appear in the profiles in the north (profiles 1, 2; **Fig. 3A**) and the southeast (profiles 4, 5). Larger wavelengths (200-800 m) and wave heights (8-38 m) are found in the profiles in the west (profiles 7, 8) (**Fig. 3B**) and the south (profile 9) (**Fig. 3D**). Profile 6 in the southwest shows the longest wavelengths (700-1,200 m) and highest wave heights (28-62 m).

Ultra-high resolution AUV bathymetry allows for imaging of USBs on the northeastern flank of Santorini in great detail (**Fig. 4**). Here, we identify several concave USBs that extend from the shelf of Santorini towards the Anhydros Basin and form several large steps that we interpret as slumps (**Fig. 4**). Toward Santorini, there is a distinct, near-vertical cliff that is variably exposed, which we interpret to be the island shelf break. The USBs lie below this cliff and appear to be the result of mass movement across the cliff, which allows classifying them as type 2 USBs (slope-failure related) following Pope et al. (2018). We identify numerous blocks on the seafloor with diameters ranging from 2-15 m (see enlargements in **Fig. 4**). In addition, we identify several pockmarks with

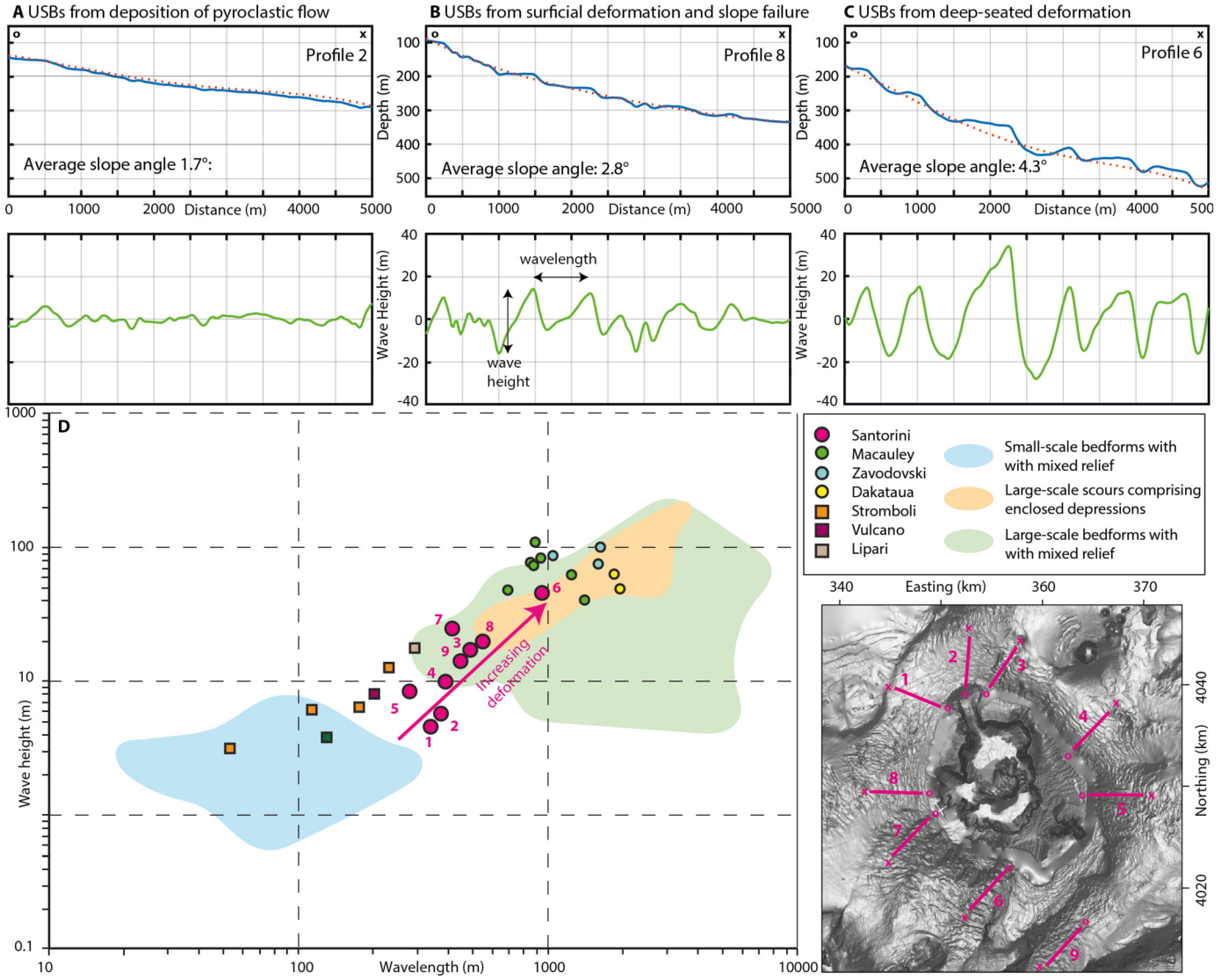

Fig. 3. (A)–(C) Morphological profiles of Santorini's flanks (blue line), regression curves through these profiles (dotted red line), and difference of both (green line) showing the wavelength and wave height of USBs. Profile 2 shows subtle USBs related to pyroclastic flows to the north (A), profile 8 shows medium-scale USBs associated with slope failures to the west (B), and profile 6 shows large-scale USBs associated with deep-seated deformation (C). (D) Comparison of wave height and wavelength of USBs around Santorini versus USBs around other volcanoes based on Pope et al. (2018) and Casalbore et al. (2021).

diameters of 20-35 m and depths of ~2 m that could be the result of degassing from the volcanoclastic sediments (**Fig. 4**).

4.2. Seismic interpretation of USB structures

According to Preine et al. (2022a), the seismic stratigraphy of the basins around Santorini comprises six units of Plio-Pleistocene age (**Figs. 5, 6**). The sediments within the uppermost Unit 6 consist of volcaniclastic deposits of the TPF, while Unit 5 is interpreted to consist mainly of hemipelagic sediments (Preine et al., 2022a). Towards the flanks of Santorini, interpretations of the stratigraphy become ambiguous since deeper units fade out. In contrast, the shallowest units have been deposited by the 3.6 ka Minoan and 22 ka Cape Riva caldera-forming eruptions (Karstens et al., 2023). Seismic profile I extends from the northern caldera breach of Santorini towards the Ios shelf (**Fig. 5A**). The red horizon marks the shallowest unit around Santorini, interpreted as Minoan ignimbrite, which is erosive at the slope of the caldera but becomes conformable towards the Ios shelf (Karstens et al., 2023). The internal reflections are wavy and stacked upon each other, with some internal reflections indicating the thrusting of material (**Fig. 5A**). The blue horizon (h6) marks the base of Unit 6, which consists of a series of wavy or chaotic seismic subunits forming a thick (~350 m) wedge that comprises the eruptive products of the TPF (Preine et al., 2022a); the green horizon marks a prominent internal horizon of Unit 6 (**Fig. 5A**).

Seismic profile II extends from the northern flank of Santorini towards the northeastern Christiana Basin (**Fig. 5B**). The Ios shelf forms a ridge separating the profile into two domains. To the east, we identify the same units described for profile I and TPF deposits of Unit 6 reach a thickness of ~200 m with the Minoan Unit lying conformably on top (**Fig. 5B**). The profile direction is parallel to the local USB trend explaining the lack of surface undulation (**Fig. 5B**). West of the ridge, Unit 6 is significantly thinner (~50 m) or even absent which is the result of a seafloor failure comprising material of Unit 6 with horizon h6 acting as glide plane (**Fig. 5B**). The failed material was transported from the headwall over several kilometers forming a chaotic mass transport deposit (MTD) on top of undisturbed sediments from Unit 6 (see enlargements in **Fig. 5B**). The exposed glide plane and the translated blocks as well as the MTD cause an undulating seafloor expression (**Fig. 5B**). Seismic profile III covers a 5-km-wide channel connecting

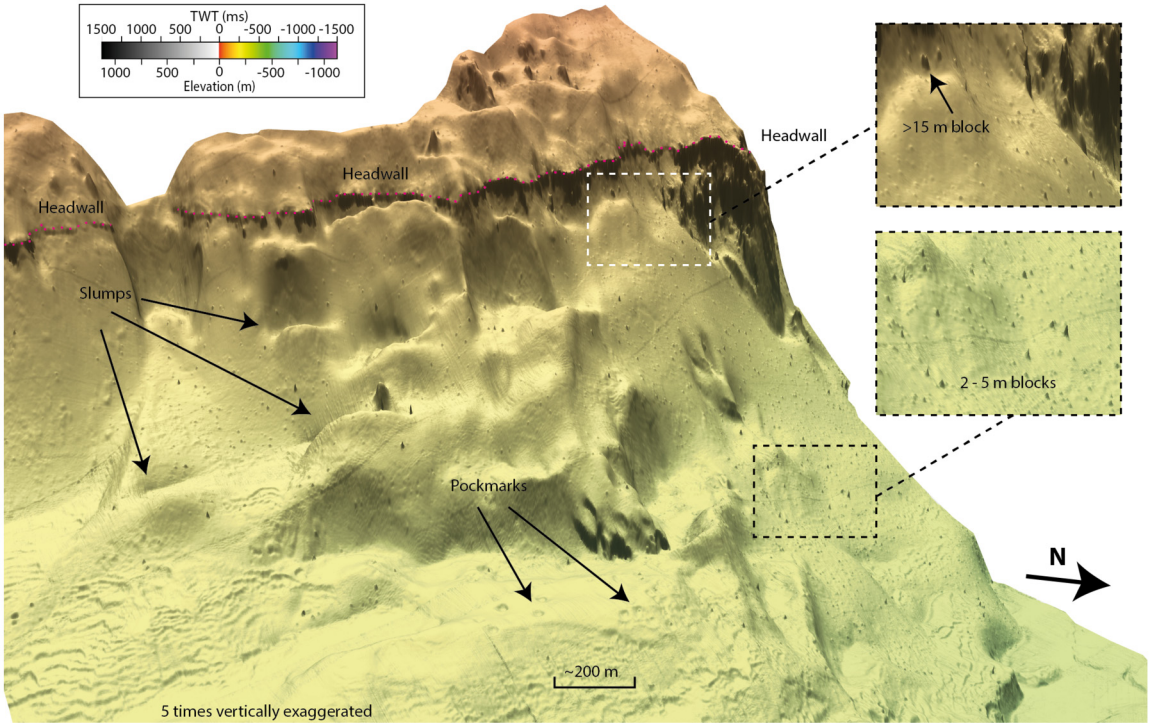

Fig. 4. 3D view of high-resolution AUV bathymetry covering the northeastern slope of Santorini. The bathymetry shows marine ignimbrites from the Minoan eruption slumped from the island's shelf into the neighboring Anhydros Basin. Enlargements show multi-meter-scale blocks that have been transported by the pyroclastic flows of the Minoan eruption.

the Santorini-Anafi Basin with the Cretan Basin south of Santorini (**Fig. 5C**). Upslope, the shallow stratigraphy comprising Units 5 and 6 is characterized by well-stratified sediments, while Unit 6 is affected by strong deformation further downslope (**Fig. 5C**). In this area, there is no seismically resolvable layer that can be associated with the Minoan eruption. The deformation causes a highly complex internal structure and appears to be a combination of extensional and compressional deformation leading to the undulating seafloor morphology.

Seismic profile IV extends from the western caldera breach into the Christiana Basin, where the TPF/Unit 6 has a thickness of ~50 m, with the Minoan deposits representing a flat and conformable subunit (**Fig. 6A**). In contrast, towards Santorini, sediments comprising Unit 6 (and possibly 5) are strongly deformed. Further upslope at profile-kilometers 13-15, large-scale USBs appear to be the surface expression of rotated blocks (**Fig. 6A**). Further south, the seismic profile extends from Santorini towards the southeastern part of the Christiana Basin terminating against the Christiana edifice (**Fig. 6B**). Similarly, there is a pronounced contrast of the internal architecture of Unit 6 with well-stratified reflections in the southwestern part and strongly deformed sediments on the foot of the flank of Santorini (profile-km 8-13, **Fig. 6B**). The transition from both facies is highlighted by the enlargements which shows that the deformation affects both Unit 6 and Unit 5. Deformation at the flank is extensional with rotated blocks (profile-km 12-14, **Fig. 6B**), while thrust structures indicate a compressional regime at the toe of the deformed flank segment (**Fig. 6B**).

Profiles VI and VII cross the southeastern margin of the Christiana Basin and highlight the pronounced flank deformation in this area (**Fig. 6C, D**). The profiles are oriented parallel to the slope direction (**Fig. 6C, D**). While profile VI shows an intact and undeformed slope segment (**Fig. 6C**), profile VII covers a failed slope segment less than 2 km apart (**Fig. 6D**). The undeformed slope segment consists of well-stratified sediments on the upper flanks; there is no indication of internal deformation in this flank segment (**Fig. 6C**). In marked contrast, profile VII shows the largest amplitudes of USBs around Santorini (up to 60 m) and the distinctive step-like bedforms show a strong indication of rotational deformation, indicating an extensional regime (**Fig. 6D**). The internal architecture of the step-like bedforms here is complex and backward-tilted layers lying on a well-defined basal shear surface can be identified (h6, **Fig. 6D**).

4.3. Combination of bathymetric and seismic reflection data

We combine seismic profiles with the multibeam bathymetry to show a 3D view of the northern flank of Santorini between the northern caldera breach and the Ios shelf (**Fig. 7A**). USBs are limited to the area just behind the caldera breach and have amplitudes of 3-12 m and wavelengths of 150-400 m (**Fig. 7A**). The bathymetry highlights that the USBs have a convex shape and extend radially along the northern caldera breach (**Fig. 7A**). On the northwestern slope of Santorini towards the Christiana Basin, USBs show a concave shape and are related to the erosive surface observed in the seismic profile (**Fig. 7B, 5B**). These features have larger amplitudes (10-30 m) and larger wavelengths (200-600 m) compared to the northern flank of Santorini. Where Unit 6 is absent, the seafloor is a smooth surface, indicating that horizon h6 marks a major lithological boundary separating consolidated sediments of Unit 5 (comprising mainly hemipelagic sediments) from Unit 6 (comprising mainly volcaniclastic material from the TPF; Preine et al., 2022a). On the southwestern flank of Santorini, the rotated blocks affect large areas along the slope and mid-slope areas (**Fig. 7C**). This internal deformation affects the entire strata of Unit 6, and, strikingly, none of these large USBs are covered by seismically resolvable sediment, indicating a young formation or reactivation age of these features or preferential non-deposition (**Fig. 7C**).

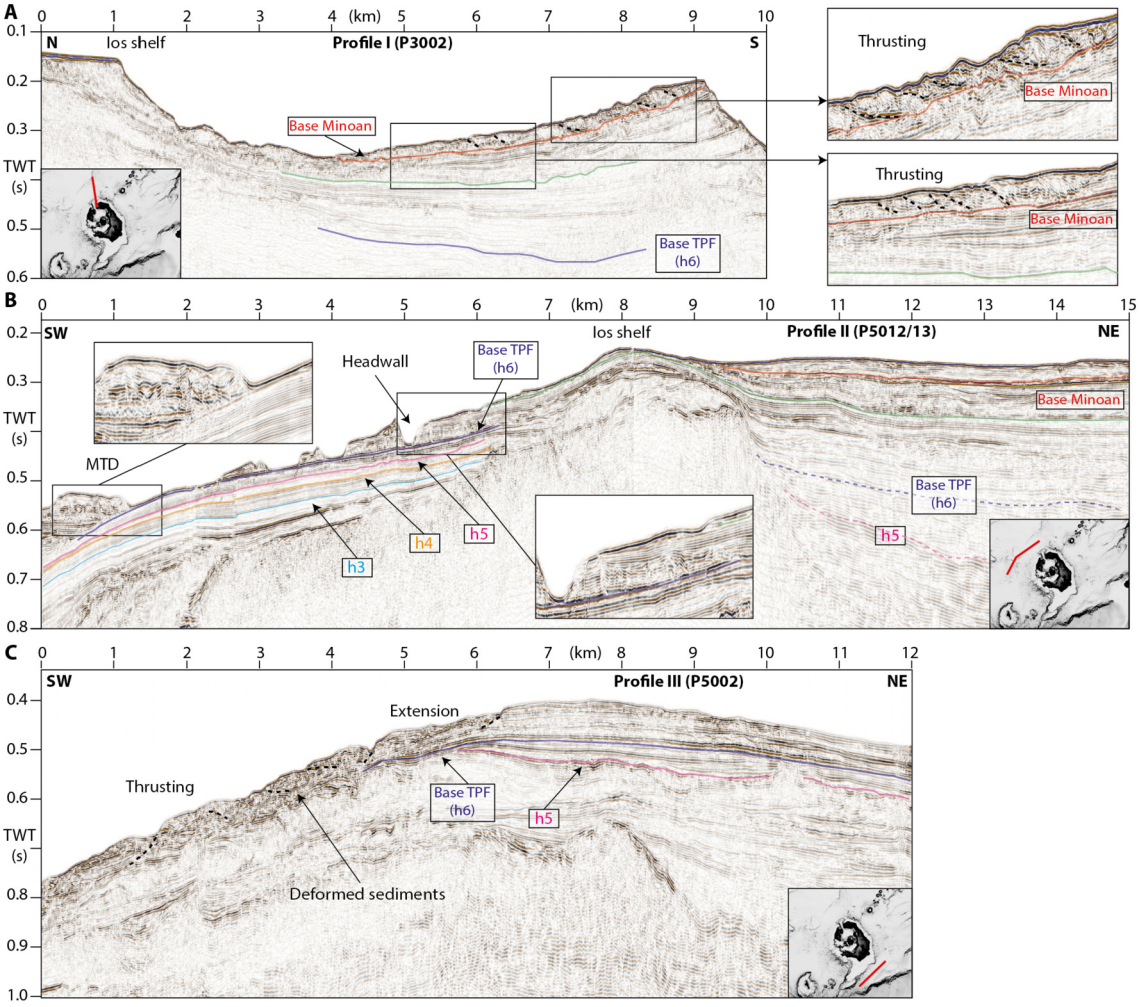

Fig. 5. (A) Seismic profile extending from the northern breach of the caldera towards the Ios shelf with enlargements highlighting the internal architecture of the shallowest seismic subunit. (B) Seismic profile between the northwestern flank of Santorini and the Ios shelf. (C) Seismic profile south of Santorini extending from the Santorini-Anafi Basin towards the Cretan Basin. Colored lines indicates key horizons as defined in Preine et al. (2022a) and Karstens et al. (2023).

5. Discussion

5.1. Characterization of large-scale undulating seafloor bedforms around Santorini

Pope et al. (2018) have identified the deposition of volcanogenic flows and gravitationally-driven slope failure as the main processes controlling the formation of USBs on the submarine flanks of volcanic complexes. According to their classification, depositional bedforms (type 1) are associated with a convex planform shape and a relatively undisturbed internal stratigraphy. Slope failure-related bedforms (type 2) have a concave to linear planform shape. They are characterized by a chaotic internal architecture with thrust faults, indicating compression at the toe of the MTD, and normal faults, indicating extension further upslope (Pope et al., 2018).

USBs are known from many other submarine volcanoes, including Macauley, Dakataua, Zavodovski, the Aeolian Islands, and the Azores (Pope et al., 2018; Casalbore et al., 2021; Chang et al., 2022). Macauley, Dakataua, and Zavodovski volcanoes are similar in size to Santorini, approximately 5-15 km in diameter, lie in island arc settings, and have had caldera-forming eruptions that discharged ~10 to 100 km^3 of tephra with pyroclastic flow generation as at least one phase of each eruption (Siebert and Simkin, 2002). USBs around these volcanoes have the largest wavelengths and wave heights **(Fig. 3D)**. On the other end of the spectrum are USBs from the Aeolian Islands, which have smaller wavelengths and wave heights (**Fig. 3D**). While volcanism at the Aeolian Islands is mainly effusive, pyroclastic flow generating eruptions are known from Lipari, Vulcano, and Stromboli (Lucchi et al., 2013).

USBs at Santorini cover a comparably wide range of the spectrum with wave heights between 1 and 80 m and wavelengths between 150 and 1,200 m and plot between the Aeolian Island USBs and those associated with large caldera-forming centers suggesting that there is likely a continuum of USBs in the wave height/wavelength domain that defines a broadly linear trend on a log/log plot (**Fig. 3D**). The smallest USB wavelengths and wave heights around Santorini are found on the northern slopes, where USBs have a convex bedform (**Figs. 2, 5, 6, 7**). The north flank of Santorini has been the main depocenter of volcaniclastics from the TPF, and it is possible to identify the base of Minoan eruption ignimbrite (**Fig. 5A, 7A**; Preine et al., 2022a; Karstens et al., 2023), that were likely deposited by pyroclastic flows (Druitt et al., 1999, 2019b; Johnston et al., 2014). Therefore, this deposit and its surficial USBs are flow-derived depositional structures per definition (type 1 following Pope et al. (2018)). However, their internal architecture and seismic characteristics differ significantly from typical type 1 units as the Minoan ignimbrite has a somewhat chaotic internal architecture with coherent internal reflections indicating thrust faults that control the extent and location of surface undulations. On the scale of the seismic resolution, there is no evidence of internal anti-dune-like structures resulting from bedload deposi-

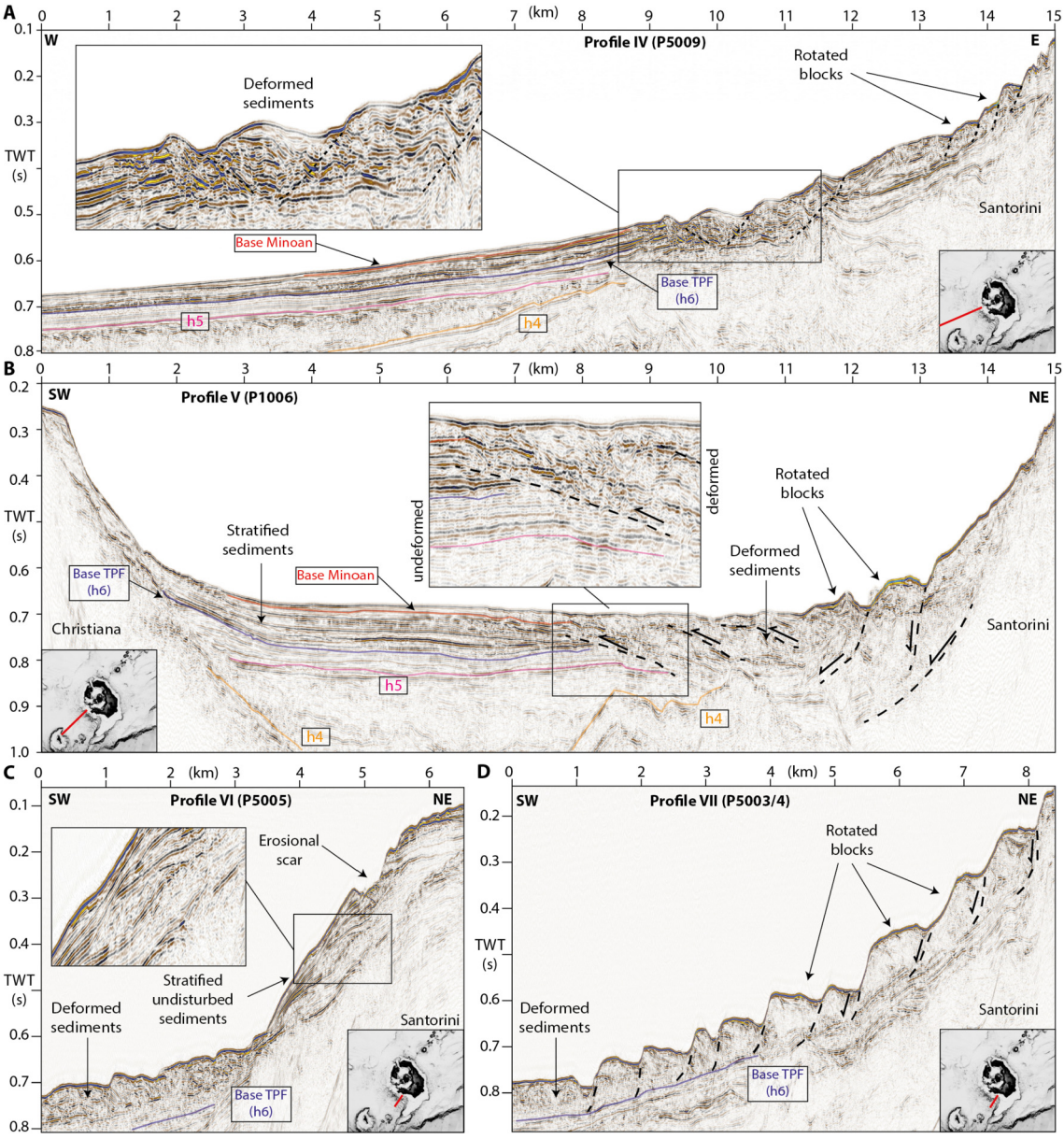

Fig. 6. Seismic profiles from the western and southwestern flanks of Santorini. (A) Seismic profile extending from the western caldera breach towards the Christiana Basin. The enlargement highlights an area of distinct internal deformation. (B) Seismic profile between Santorini and Christiana. The enlargement highlights a transitional zone between laminated and highly disturbed seismic facies of Units 5 and 6. (C), (D) Seismic profiles extending from the southwestern flank of Santorini towards the southwest with little (C) and intense (D) internal deformation.

tion (**Figs. 5A, 7A**). Therefore, USBs north of Santorini define a new sub-class of bedforms (e.g., type 1B) that should be added to the classification scheme of Pope et al. (2018).

Along Santorini's northeastern, western, and southwestern slopes, the USBs' wavelengths and wave heights increase, and seismic profiles show a significant deepening of deformation beneath the USBs (**Fig. 8A-C**). To the southwest of Santorini, linear USBs have the largest wavelengths and wave heights (**Figs. 3D, 6C, 7C**) and have similar dimensions as those found around other volcanoes affected by caldera-forming eruptions (**Fig. 3D**). USBs in this area are the surface expression of km-scale rotated blocks, thrust structures, and heavily deformed sediments. To the south, east, and west of Santorini, the planform shape of the USBs is concave to linear (**Fig. 2**), and the deformation affects mainly the TPF with normal faults indicating extension in the upper slope of the profiles (**Figs. 5C, 6**). Their seismic stratigraphy and planform shape indicate slope failure as the governing formation process following the classification scheme of Pope et al. (2018). The AUV bathymetry underscores this interpretation from the northeastern flank of Santorini, where we can identify a distinct headwall and related slumps (**Fig. 4**). This scar seems to be related to a former shelf break, likely consisting of lava flows from the Peristeria volcano, which defines the morphology of the northeastern side of Santorini (**Fig. 2**) (e.g., Druitt et al., 1999).

Profile V covers an area within the northwestern USBs resulting from a slope failure with upslope extension and compression at the toe (**Fig. 6B**). The fact that a seismically resolvable unit covers neither this area nor the USBs elsewhere suggests that the observed slope instabilities were active during or after the deposition of the Minoan ignimbrite, which is also highlighted by the presence of large blocks in the AUV bathymetry (**Fig. 4**). The USBs to the south (profile 9; **Fig. S1I**), east (profile 8, **Fig. 3B**) and west (profile 4, **Fig. S1D**) of the island have intermediate wavelengths and wave heights (**Fig. 3D**) and have concave surface bedforms.

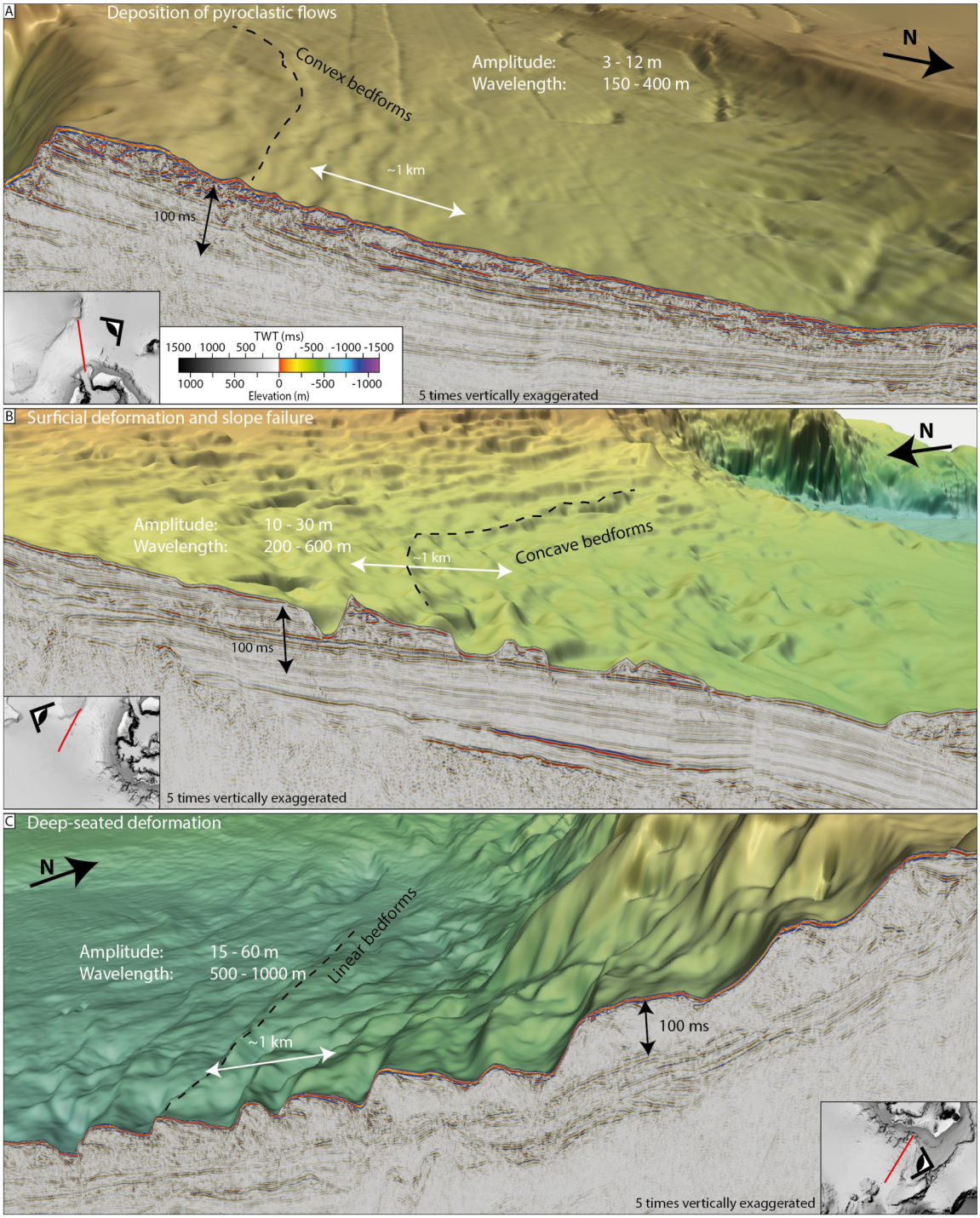

Fig. 7. 3D views on seismic profiles combined with morphological grids of the slopes of Santorini. (A) Northern slope of Santorini viewed from the east. The rim of the northern caldera breach is visible on the left side. Small-scale USBs extend behind the breach. Seismic profile corresponds to Fig. 5A. (B) Northwestern flank of Santorini viewed from the northwest. Irregular USBs are related to slope failures of the TPF. Seismic profile corresponds to Fig. 5B. (C) Southwestern flank of Santorini viewed from the south. USBs are related to rotated blocks. Seismic profile corresponds to Fig. 6D.

The comparison of USBs at Santorini indicates that USBs become larger with increasing internal deformation (**Fig. 3D**). The TPF has a thickness of 300 ms TWT on Santorini's northern flank (Fig. 5A), where USBs have the smallest dimensions, while the thickness of the TPF is less than half on all other flank segments, where USB dimensions are larger. However, these flank segments have steeper slope angles compared to the northern flank, which is considered a critical feature, as slope angle directly affects the safety factor favoring slope failure at the steepest part of the slope in response to gravity and seismic loading (Puzrin et al., 2015). This is in agreement with observations at Santorini, where the most pronounced USBs develop at the northeastern and southwestern flanks (Figs. 4–7), where the slope is the steepest, and with observations from other geological settings indicating that slope angle is the dominant factor for slope stability (Miramontes et al., 2018).

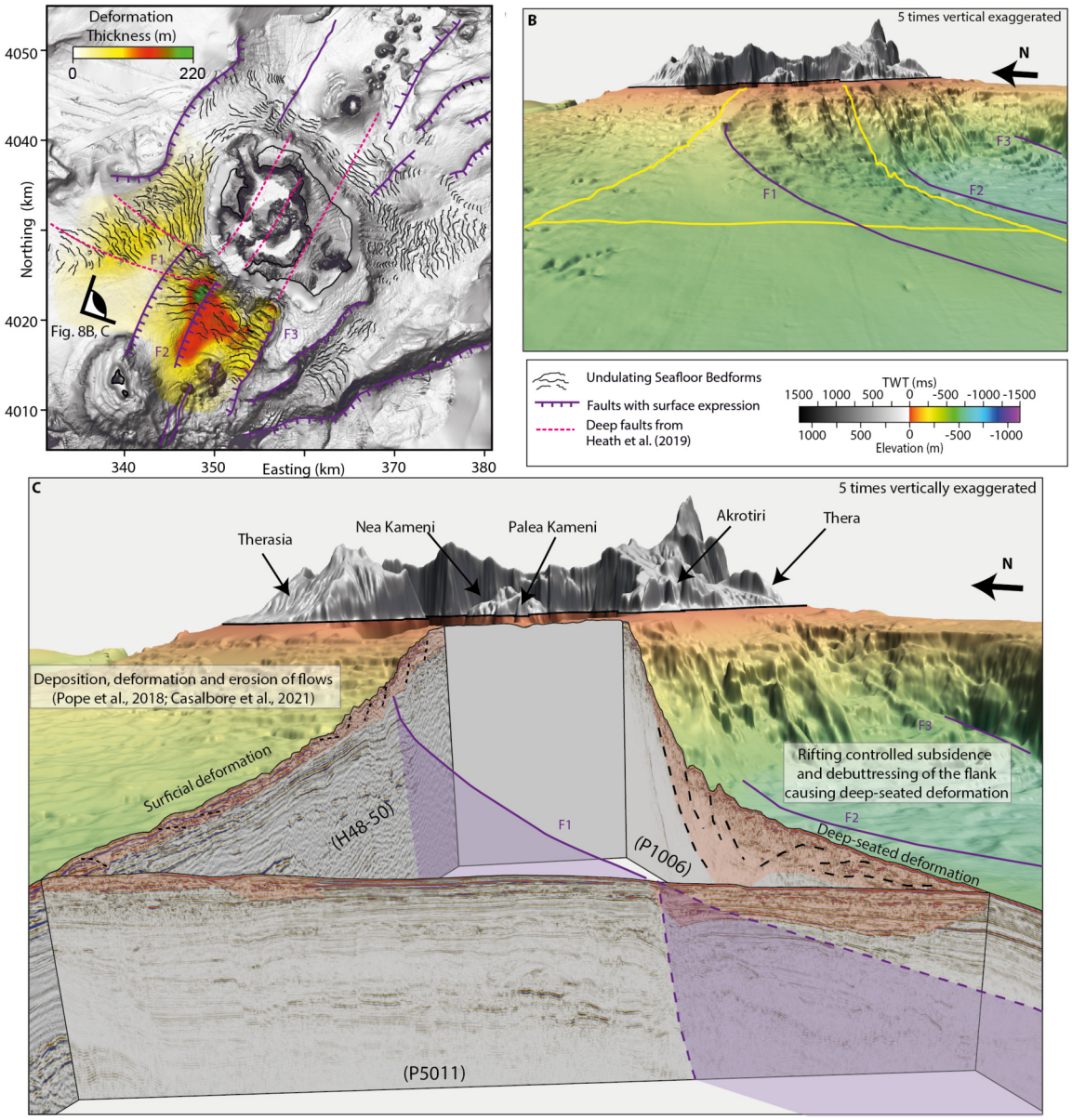

Fig. 8. (A) Morphological map of Santorini highlighting USBs, major surficial faults from Nomikou et al. (2018) and Preine et al. (2022a), deep faults from Heath et al. (2019), as well as the thickness of the deformation. 3D view on the southwestern flank of Santorini from the Christiana basin with major faults and seismic profiles shown in (C). (C) 3D view from the same viewpoint combining seismic profiles and bathymetry illustrating how deformation deepens towards the southeast correlating with major faults. Profile H48-50 is from another survey (POS338; Hbscher et al., 2006). See Preine et al., 2022b for acquisition and processing details.

5.2. Formation of undulating seafloor bedforms during the Minoan eruption

5.2.1. Entrance of Pyroclastic flows into the Sea

Caldera-forming eruptions like the Minoan event can generate enormous volumes of volcaniclastic sediment reaching up to hundreds of cubic kilometers of material (e.g., Carey and Sigurdsson, 1989; Legos and Druitt, 2000; Freundt, 2003). The material can be delivered to the marine environment by fallout through the water column, or sediment gravity flows that typically originate as pyroclastic flows and surges (Carey and Schneider, 2011). There is only limited information about the timing and duration of pyroclastic flow discharge at Santorini. Still, a recent seismic analysis suggests that the volume may have been as much as 6.9 $\pm$ 2 km^3 DRE of pyroclastic material (Karstens et al., 2023). Such a large volume of volcaniclastics entering the sea, essentially instantaneously, would have had a significant impact on the seafloor. The analysis of sediment cores around Santorini indicates the presence of ground-based flow deposits extending tens of kilometers towards the east of Santorini, deposited before co-ignimbrite ash settled on top (Karstens et al., 2023). This suggests that pyroclastic flow discharge occurred over hours rather than weeks indicating that pyroclastic flow discharge rates of the Minoan eruption and the 1883 Krakatau eruption, during which 14 km^3 of dacitic magma were deposited over the period of one day (Sigurdsson et al., 1991a,b), likely were similar.

At Krakatau, major underwater pyroclastic flows formed a deposit up to 80 m thick that extended up to 80 km from the volcano (Carey et al., 1996). The presence of USBs at Krakatau is currently unknown due to a lack of high-resolution bathymetric data. An omnidirectional deposition of pyroclastic flows during the Minoan eruption can be inferred from the great thicknesses of onshore pyroclastic flow deposits on the coasts of Santorini, where enormous volumes of pumice and ash must have entered the sea (Druitt et

al., 2019b). This agrees with analogue volcanic jet experiments of the collapse of a particle-laden plume to simulate pyroclastic flow formation resulted in the deposition of concentric sediment ridges around the plume source resembling the USBs observed at Santorini (Gilchrist and Jellinek, 2021; Gilchrist et al., 2023). These authors suggested that the sediment waves surrounding Santorini may have formed by concentric discharge of material during plume collapse. Our results do not support the notion that the Santorini USBs are purely depositional in nature, as we describe below.

The seismic stratigraphy of Minoan deposits to the north of Santorini allows an analysis of the depositional processes controlling USB formation (**Figs. 5A and 7A**). USBs of the northern deposit fan correlate with internal thrust structures, indicating a compressional regime at the toe of the slide (Frey-Martínez et al., 2006). Such structures are often found in spatially confined MTDs worldwide (e.g., Sakar Island, Kühn et al., 2021 or offshore Montserrat, Watt et al., 2012). However, the Minoan ignimbrite was emplaced unconfined in the north, and we suggest that thrusting developed as the result of loss of kinematic energy during emplacement (Frey-Martínez et al., 2006), causing the leading flow segment to decelerate due to interaction with the substrate and the following material to push into it (**Fig. 8B**). These USBs have the smallest wave heights and shortest wavelengths of all USBs around Santorini (**Fig. 3**).

5.2.2. Instability of volcaniclastic deposits

Apart from the northern flank, nearly all USBs around Santorini result from deformation processes, i.e., slope failures. Earthquakes generate horizontal and vertical accelerations that increase shear and normal stresses and therefore are possible triggers for such deformation (Hampton et al., 1996). Strong, shallow earthquakes are a common feature associated with large-scale explosive eruptions, especially when the foundering of the volcanic edifice leads to the generation of a caldera (Yokoyama, 2001; Stix and Kobayashi, 2008). Earthquakes with magnitudes of 7 have been inferred for the 1815 eruption of Tambora in Indonesia and the 1912 eruption of Mt. Katmai in Alaska (Yokoyama, 2001; Abe, 1992). More recently, the smaller eruption of Mt. Pinatubo in 1994 was associated with an earthquake of magnitude 5.7 (Mori et al., 1994), and a correlation between earthquake magnitude and caldera collapse volume has been suggested (Abe, 1979). During the Minoan eruption, the caldera floor dropped by almost 600 m (Johnston et al., 2014) with a caldera collapse volume of ~33 km^3 (Karstens et al., 2023). Significant earthquakes likely accompanied this event.

Hurlimann and Marti (2000) analyzed the magnitude of an earthquake necessary to generate significant slope failure on the sides of a caldera-forming volcanic center. They calculated that even a comparably small earthquake with magnitude Mw 5 centered at a caldera could trigger slope failures. Although such calculations are difficult to generalize or to transfer to Santorini directly as slope angle, shear strength and thickness of sediments control slope stability, it appears plausible that seismic shaking was a contributing factor in the formation of deformational USBs at Santorini. Type 2 USBs, including those around Santorini, share morphological characteristics known from subaqueous MTD affected by spreading (e.g., the Storegga Slide), which in many cases are triggered by earthquakes causing liquefaction or strain softening along a lithologically defined glide plane (Micallef et al., 2007; Bucci et al., 2022). The boundary between the TPF and the underlying hemipelagic sediments northwest (h6 in **Fig. 5B**; Preine et al., 2022a) or older lava flows northeast of Santorini (**Fig. 4**) appears to have acted as glide planes for USBs related to surficial deformation around Santorini. The mainly pyroclastic deposits of the TPF are expected to have a low effective stress governed by the low density of pumice clasts (Wiemer and Kopf, 2017). The combination of intense seismic shaking and rapid deposition of large amounts of material on top of deposits of low shear strength on steep slope gradients can explain the formation of slope instabilities and the creation of deformational USBs around Santorini during the Minoan eruption (**Fig. 9B, C**). Evidence for this process can be observed to the south, east, and west of Santorini, where slope failure, even locally, caused an evacuation of the slide plane (**Figs. 5B, 7B**) or exposed the headwall (**Fig. 4**). These USBs have larger dimensions than those primarily attributed to deposition of pyroclastic flows (Fig. 3).

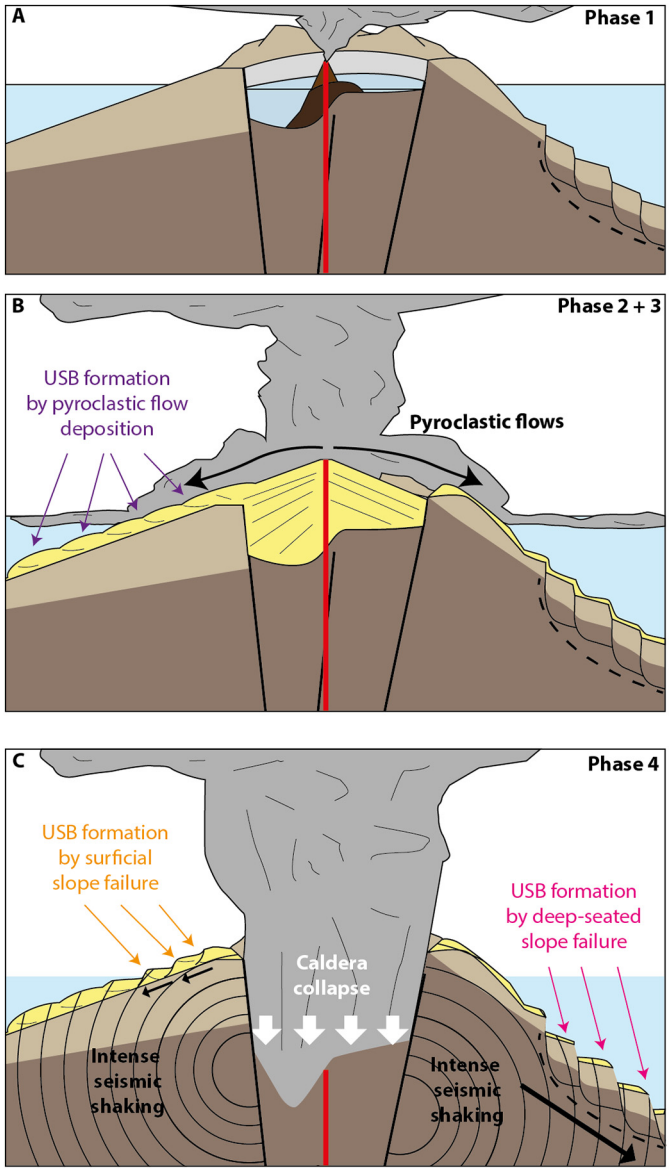

Fig. 9. Illustration of the development of USBs on Santorini's flank. (A) Phase 1 of the eruption initiated with a subaerial eruption from an onshore vent in the Caldera (Druitt et al., 2019b) with pre-exiting deep-seated deformation at the southern flank. (B) Deposition of pyroclastic flows during Phases 2 and 3 of the eruption forming depositional USBs on the northern flank of the island. (C) Caldera collapse during Phase 4 of the eruption triggering slope instabilities and reactivating deep-seated deformation.

5.2.3. Deep-seated deformation of the volcanic edifice

In terms of sediment depth, the deformation of volcanic deposits on the northwestern flank of Santorini is comparably shallow, but becomes significantly deeper towards the southwestern flank of the island (**Fig. 8A**). The lateral extent of this deep-seated deformation correlates with the Christiana Fault (F1 in **Fig. 8B**),

which stretches from the sidewall of a sector collapse at Christiana (Preine et al., 2022b) towards the northeast and continues on the western slope of Santorini. This fault correlates with a topographic step in the seafloor (**Figs. 2, 8**). It defines the boundary between an area with smooth morphology with minor USBs to the NW and a significantly more rugged terrain with large amplitude/wavelength USBs to the SE in the Christiana Basin (**Figs. 2, 8**). This morphology results from extension along rotational normal faults on Santorini's slope and a compressional regime leading to thrusts in the Christiana Basin (**Figs. 6B, 6C**). Towards the southwest, an additional morphological step coincides with faults (F2) controlling the segmentation of Christiana Basin sedimentary infill (Preine et al., 2022b). A major normal fault (F3) defines the southeastern boundary of the Christiana Basin (**Fig. 8**) following the regional SW-NE fault trend (Hooft et al., 2017; Nomikou et al., 2018; Preine et al., 2022c). This suggests that rift tectonics affect the slopes of Santorini and control the deep-seated deformation, which is only observed in front of the southwestern flanks of the volcanic edifice. Strikingly, this area between Santorini and Christiana marks the intersection of the former Pliocene ESE-WNW striking tectonic regime and the new NE-SW directed fault trend that emerged in Early Pleistocene and shaped the Santorini-Amorgos Tectonic Zone northeast of Santorini (Heath et al., 2019; Preine et al., 2022c). This new fault trend seems to continue underneath Santorini, and the intersecting fault trends define the area affected by deep-seated deformation (**Fig. 8**; Heath et al., 2019; Preine et al., 2022c).

Deep-seated deformation within volcanic edifices is known from many volcanoes worldwide, including Mount Etna, Kilauea, and Piton de Fournaise, where the interplay between volcanic rifts, gravitational instability, and regional tectonics appear to play a significant role (Poland et al., 2017). In the case of Etna, deformation controlled by major fault systems is an active process measured in the onshore and offshore domains that appear to occur (at least temporally) independent from volcanic activity (Urlaub et al., 2018). Deep-seated deformation of volcanic edifices received major attention with the 2018 sector collapse of Anak Krakatau, for which the analysis of Interferometric Synthetic Aperture Radar (InSAR) revealed that the volcanic edifice slowly deformed before the catastrophic collapse (Walter et al., 2019). Similar observations have been made for the 1888 Ritter Island sector collapse based on seismic data (Karstens et al., 2019), where deep-seated deformation caused instability of the volcanic edifice that formed USBs with thrust structures similar to those observed in the Christiana Basin. At Ritter Island, a small volcanic cone buttressed the actively deforming flank and caused the formation of a stable toreva block separating the two catastrophically failed flank segments (Karstens et al., 2019). The active opening and thus extension of the Christiana Basin likely has had a contrasting effect, resulting in debuttressing and facilitating structural instability of Santorini's southwestern flank. The USBs at this flank segment have the by far largest wave heights and wavelengths of all bedforms around Santorini indicating a direct correlation between internal deformation and slope angles with USB dimensions (Fig. 3).

The increase of deformation with depth suggests that deep-seated deformation at Santorini is a long-term process that initiated before the Minoan eruption. Previous major caldera collapses like that during the 21 ka BP Cape Riva eruption and ground acceleration associated with major tectonic earthquakes in neighboring rift basins had likely a significant impact on the development of the observed slope instabilities (**Fig. 9C**). Since there is no evidence for seismically resolvable draping of the USBs their formation or reactivation occurred during or after deposition of the Minoan deposits. This suggests that a major pulse of deep-seated deformation likely accompanied caldera collapse during the Minoan eruption.

5.3. Implications for slope stability and geohazard assessment at Santorini

The Minoan eruption is associated with a significant tsunami, whose deposits have been identified on the surrounding islands, on the northern coast of Crete, and as far as Turkey and Israel (Bruins et al., 2008; Novikova et al., 2011; Lespez et al., 2021; Paris et al., 2022). There is an ongoing debate about the tsunami source mechanisms during the Minoan eruption, with caldera collapse and the emplacement of pyroclastic flows being the primary candidates in the publications above. At the same time, slope instabilities have not received much attention because they were not resolved before this study. Here, we suggest that the slope instabilities on the flank of Santorini formed or have been reactivated during the Minoan eruption. Such widely distributed deformation likely would have had a significant tsunami potential as demonstrated by the sector collapse of Anak Krakatau in 2018, during which a comparably small slide volume of $\sim$0.3 km^3 triggered a devastating tsunami at the coasts surrounding the Sunda Strait (Grilli et al., 2019). The deep-seated deformation between F2 and F3 alone affects sediments with a volume of $\sim$2 km^3 (**Fig. 7**). Considering that type 2 USBs are found on all sides of Santorini in shallow water depths of less than 500 m implies a significant tsunami potential during USB formation. We suggest that a combination of slope instabilities and the potential simultaneous deposition of 6.9 $\pm$ 2 km^3 DRE of pyroclastic material (Karstens et al., 2023) could explain the large size of the Minoan tsunami. Bathymetric data from Hunga Tonga Hunga Ha'apai (HTHH) show indications for USBs on the flank of the volcano and in the neighboring basin (Seabrook et al., 2023). The USBs on the eastern flank of HTHH have a wave height of $\sim$70 m and a wavelength of 1 to 2 km and thus have similar dimensions as those associated with deep-seated deformation at Santorini. Whether this is a result deep-seated syn-eruptive deformation of the flanks of HTHH remains speculative until seismic reflection data is available.

Except for a phase of unrest accompanied by inflation from 2011 to 2012, the Santorini caldera floor is experiencing subsidence (Parks et al., 2015) and there are currently no indications for magma migration in the underground. However, catastrophic collapses of unstable volcanic flanks are not always related to volcanic activity (Van Wyk de Vries and Francis, 1997). Santorini is located in one of Europe's most tectonically-active regions, which hosted the tsunamigenic 1956 Mw 7.5 and 7.2 earthquakes (Brüstle et al., 2014). If an earthquake with a similar magnitude occurred in the direct vicinity of the Santorini edifice, ground acceleration could reactivate the surficial slope instabilities surrounding Santorini, particularly on the southwest flank. At Kilauea, intense slip along the detachment of the Hilina slump was repeatedly associated with large-scale earthquakes like the 2018 Mw 6.9 and the tsunamigenic 1975 Mw 7.7 earthquakes (Lin and Okubo, 2020). The reactivation of the deep-seated deformation at Santorini's southwestern flank might have a significant, so far unrecognized tsunamigenic potential. As the zone of instability is entirely submerged, it cannot be monitored using satellite-based InSAR measurements. Additional marine seismic measurements and seafloor-based geodetic measurements like those applied at the submerged flank of Mt Etna (Urlaub et al., 2018) are required to evaluate the current state of the flank.

6. Conclusions

An integrated analysis of high-resolution seismic reflection profiles and bathymetric data led to the differentiation of three types of undulating seafloor bedforms (USBs) and their formational processes around the Santorini volcanic complex in the Aegean Sea. USBs to the north of the islands have the lowest amplitudes and

wavelengths and formed within pyroclastic flow deposits from the 3.6 ka Minoan eruption. The undulations likely result from thrusting, caused by deceleration of the leading part of submarine flows during emplacement. This represents a new sub-type of depositional bedforms, adding to the classification scheme by Pope et al. (2018). USBs to the west and northeast of Santorini are associated with slope failures that include Minoan deposits and volcaniclastic material from the entire Thera Pyroclastic Formation. These USBs and related collapse structures are not covered by material from the Minoan eruption, indicating that they have formed after the main phase of pyroclastic flow discharge. Southwest of Santorini in the Christiana Basin, USBs have the highest amplitudes and wavelengths and are associated with deep-seated deformation extending to at least 200 m below the seafloor. The deep-seated deformation spatially correlates with the intersection between Pliocene and present-day rift structures. A lack of mantling of the deep-seated USBs by Minoan deposits indicates that they have been formed, or more likely reactivated, during the Minoan eruption. Our results show that USB formation during the Minoan eruption is complex and likely the result of several processes, rather than solely being a depositional phenomenon associated with eruption column collapse (Gilchrist et al., 2023).

The common occurrence of USBs on the seafloor surrounding submarine and partially emergent calderas, particularly in subduction zone environments, suggests that specific volcanological and tectonic processes favor their formation. A characteristic feature of the undulating bedforms found on the slopes of large calderas is their radial distribution around the entire volcanic complex. Large-volume explosive eruptions that generate calderas in submarine/subaerial arc settings, such as Santorini's Minoan eruption, provide insights into the origin of concentrically distributed USBs. We suggest that a cascading series of events favor their formation during caldera-forming eruptions that include rapid loading of loose, unconsolidated pyroclastic material on submarine flanks, contemporaneous failure of such material due to associated large-scale seismic activity, and the activation of deeper-seated structural elements of complex caldera centers that are geodynamically controlled by local tectonics. The occurrence of large-scale USBs encircling a submarine or partially emergent caldera is likely to be a signature of previous large-scale explosive eruptions that have discharged tens to hundreds of cubic kilometers of magma.

From a hazard perspective, pyroclastic flow emplacement and slope failures are fundamental tsunami source mechanisms during volcanic eruptions. While the devastating tsunami associated with the Minoan eruption of Santorini has previously been attributed to the submarine emplacement of several cubic kilometers of pyroclastic flows, widespread slope failures have not been considered a tsunami source mechanism. It appears plausible that both processes acted synchronously during the Minoan eruption, which most likely increased the magnitude of the resulting tsunami. This also highlights the potential of USBs as indicators of tsunamigenic processes during past eruptions. Further combined seismic and morphologic surveys of large-scale marine volcanoes are necessary to evaluate whether the observations from Santorini can be applied to other major eruptions.

Declaration of competing interest

This project has received funding from the European Research Council (ERC) under the European Union's Horizon 2020 research and innovation programme (grant agreement No. 948797) and by the Helmholtz Association's Initiative and Networking Fund (Young Investigator Group) VH-NG-1617.

The authors have no relevant financial or non-financial interests to disclose.

Data availability

The seismic reflection profiles obtained doing POS538 are available at https://doi.pangaea.de/10.1594/PANGAEA.956579.

Acknowledgements

We want to thank the captain, crew, and scientific party of the R/V *Poseidon* POS538 expedition for their assistance in completing bathymetric and seismic surveying around the Santorini volcanic complex. We thank Mark Hannington and Sven Petersen for providing access to the AUV bathymetry dataset. In addition, we are grateful to Schlumberger for providing VISTA seismic processing software and IHS for providing KINGDOM seismic interpretation software. We want to thank Emilie Hooft and the PROTEUS project, the EMODnet consortium, and ASTER for providing the DEM data used in this study. Jonas Preine's contribution was supported by the German Research Foundation DFG (HU698/25). This project has received funding from the European Research Council (ERC) under the European Union's Horizon 2020 research and innovation programme (grant agreement No. 948797) and by the Helmholtz Association's Initiative and Networking Fund (Young Investigator Group) VH-NG-1617.

Appendix A. Supplementary material

Supplementary material related to this article can be found online at https://doi.org/10.1016/j.epsl.2023.118215.

References

Abe, K., 1979. Magnitudes of major volcanic earthquakes of Japan 1901 to 1925. J. Fac. Sci., Hokkaido Univ., Ser. 7 6 (1), 201–212.
Abe, K., 1992. Seismicity of the caldera-making eruption of Mount Katmai, Alaska in 1912. Bull. Seismol. Soc. Am. 82, 175–191.
Bell, K.L.C., 2011. On the Origin of Submarine Sediment Features in the Southern Aegean Sea. University of Rhode, Island.
Bell, K.L.C., Carey, S.N., Nomikou, P., Sigurdsson, H., Sakellariou, D., 2013. Submarine evidence of a debris avalanche deposit on the eastern slope of Santorini volcano, Greece. Tectonophysics 597, 147–160.
Bond, A., Sparks, R.S.J., 1977. The Minoan eruption of Santorini, Greece. J. Geol. Soc. (Lond.) 132, 1–16.
Bruins, H.J., MacGillivray, J.A., Synolakis, C.E., Benjamini, C., Keller, J., Kisch, H.J., et al., 2008. Geoarchaeological tsunami deposits at Palaikastro (Crete) and the Late Minoan IA eruption of Santorini. J. Archaeol. Sci. 35 (1), 191–212.
Brüstle, A., Friederich, W., Meier, T., Gross, C., 2014. Focal mechanism and depth of the 1956 Amorgos twin earthquakes from waveform matching of analogue seismograms. Solid Earth 5 (2), 1027–1044.
Bucci, M.G., Micallef, A., Urlaub, M., Mountjoy, J., Barrett, R., 2022. A global review of subaqueous spreading and its morphological and sedimentological characteristics: a database for highlighting the current state of the art. Geomorphology 108397.
Carey, S.N., Schneider, J.L., 2011. Volcaniclastic processes and deposits in the deep-sea. In: Huneke, H., Mulder, T. (Eds.), Deep-Sea Sediments. In: Developments in Sedimentology, vol. 63. Elsevier, pp. 457–515, Chapter 7.
Carey, S.N., Sigurdsson, H., 1989. The intensity of plinian eruptions. Bull. Volcanol. 51, 28–40.
Carey, S.N., Sigurdsson, H., Mandeville, C., Bronto, S., 1996. Pyroclastic flows and surges over water: an example from the 1883 Krakatau eruption. Bull. Volcanol. 57, 493–511.
Cartigny, M.J., Postma, G., Van den Berg, J.H., Mastbergen, D.R., 2011. A comparative study of sediment waves and cyclic steps based on geometries, internal structures and numerical modeling. Mar. Geol. 280 (1–4), 40–56.
Chang, Y.C., Mitchell, N., Quartau, R., Hübscher, C., Rusu, L., Tempera, F., 2022. Asymmetric abundances of submarine sediment waves around the Azores volcanic islands. Mar. Geol. 449, 106837.
Casalbore, D., Clare, M., Pope, E., Quartau, R., Bosman, A., Chiocci, F., Romagnoli, C., Santos, R., 2021. Bedforms on the submarine flanks of insular volcanoes: new insights gained from high resolution seafloor surveys. Sedimentology 68, 1400–1438.
Druitt, T., Edwards, L., Mellors, R., Pyle, D., Sparks, R., Lanphere, M., Davies, M., Barriero, B., 1999. Santorini Volcano. Geological Society Memoir, vol. 19. The Geological Society, London.

Druitt, T., Pyle, D., Mather, T., 2019a. Santorini volcano and its plumbing system. Elements 15, 177–184.
Druitt, T., McCoy, F., Vougioukalakis, G., 2019b. The Late Bronze Age Eruption of Santorini volcano and its impact on the Ancient Mediterranean World. Elements 15, 185–190.
Freundt, A., 2003. Entrance of hot pyroclastic flow into the sea: experimental observations. Bull. Volcanol. 85, 144–164.
Frey-Martínez, J., Cartwright, J., James, D., 2006. Frontally confined versus frontally emergent submarine landslides: a 3D seismic characterisation. Mar. Pet. Geol. 23 (5), 585–604.
Friedrich, W.L., Kromer, B., Friedrich, M., Heinemeier, J., Pfeiffer, T., Talamo, S., 2006. Santorini eruption radiocarbon dated to 1627-1600 B.C. Science 312, 548.
Gilchrist, J., Jellinek, A., 2021. Sediment waves and the gravitational stability of volcanic jets. Bull. Volcanol. 83, 64. https://doi.org/10.1007/s00445-021-01472-1.
Gilchrist, J.T., Jellinek, A.M., Hooft, E.E., Wanket, S., 2023. Submarine terraced deposits linked to periodic collapse of caldera-forming eruption columns. Nat. Geosci., 1–8.
Grilli, S.T., Tappin, D.R., Carey, S., Watt, S.F., Ward, S.N., Grilli, A.R., et al., 2019. Modelling of the tsunami from the December 22, 2018 lateral collapse of Anak Krakatau volcano in the Sunda Straits, Indonesia. Sci. Rep. 9 (1), 1–13.
Hampton, M.A., Lee, H.J., Locat, J., 1996. Submarine landslides. Rev. Geophys. 34, 33–59.
Hannington, M.D., 2018. RV POSEIDON Fahrtbericht/Cruise Report POS510-ANYDROS: Rifting and Hydrothermal Activity in the Cyclades Back-Arc Basin, Catania (Italy)–Heraklion (Greece) 06.03.-29.03.2017.
Heath, B.A., Hooft, E.E.E., Toomey, D.R., Papazachos, C.B., Nomikou, P., Paulatto, M., et al., 2019. Tectonism and its relation to magmatism around Santorini Volcano from upper crustal P wave velocity. J. Geophys. Res., Solid Earth 124 (10), 10610–10629.
Heiken, G., McCoy Jr, F., 1984. Caldera development during the Minoan eruption, Thira, Cyclades, Greece. J. Geophys. Res., Solid Earth 89 (B10), 8441–8462.
Hooft, E.E., Nomikou, P., Toomey, D.R., Lampridou, D., Getz, C., Christopoulou, M.E., et al., 2017. Backarc tectonism, volcanism, and mass wasting shape seafloor morphology in the Santorini-Christiana-Amorgos region of the Hellenic Volcanic Arc. Tectonophysics 712, 396–414.
Hb̈scher, C., Hensch, M., Dahm, T., Dehghani, A., Dimitriadis, I., Hort, M., Taymaz, T., 2006. Toward a risk assessment of central Aegean volcanoes. Eos Trans. AGU 87 (39), 401–407. https://doi.org/10.1029/2006EO390002.
Huff, A.E., Nomikou, P., Thompson, L.A., Hooft, E.E., Walker, I.J., 2021. Applying planetary mapping methods to submarine environments: onshore-offshore geomorphology of Christiana-Santorini-Kolumbo Volcanic Group, Greece. J. Maps 17 (3), 111–121.
Hurlimann, M., Marti, J., 2000. Mechanical relationship between catastrophic volcanic landslides and caldera collapse. Geophys. Res. Lett. 27, 2393–2396.
Johnston, E.N., Sparks, R.S.J., Phillips, J.C., Carey, S., 2014. Revised estimates for the volume of the Late Bronze Age Minoan eruption, Santorini, Greece. J. Geol. Soc. 171 (4), 583–590.
Karstens, J., Preine, J., Crutchley, G.J., Kutterolf, S., van der Bilt, W., Hooft, E., Druitt, T., Schmid, F., Cederstrøm, J.M., Hübscher, C., Nomikou, P., Carey, S., Kühn, M., Elger, J., Berndt, C., 2023. Revised Minoan eruption volume as benchmark for large volcanic eruptions. Nat. Commun. 14, 2497. https://doi.org/10.1038/s41467-023-38176-3.
Karstens, J., Berndt, C., Urlaub, M., Watt, S.F., Micallef, A., Ray, M., et al., 2019. From gradual spreading to catastrophic collapse–Reconstruction of the 1888 Ritter Island volcanic sector collapse from high-resolution 3D seismic data. Earth Planet. Sci. Lett. 517, 1–13.
Karstens, J., Kelfoun, K., Watt, S.F., Berndt, C., 2020. Combining 3D seismics, eyewitness accounts and numerical simulations to reconstruct the 1888 Ritter Island sector collapse and tsunami. Int. J. Earth Sci. 109 (8), 2659–2677.
Kühn, M., Karstens, J., Berndt, C., Watt, S.F., 2021. Seismic reconstruction of seafloor sediment deformation during volcanic debris avalanche emplacement offshore Sakar, Papua New Guinea. Mar. Geol. 439, 106563.
Lee, H.J., Syvitski, J.P., Parker, G., Orange, D., Locat, J., Hutton, E.W., Imran, J., 2002. Distinguishing sediment waves from slope failure deposits: field examples, including the 'Humboldt slide', and modelling results. Mar. Geol. 192 (1–3), 79–104.
Legos, F., Druitt, T., 2000. Emplacement of ignimbrite in shallow-marine environments. J. Volcanol. Geotherm. Res. 95, 9–22.
Lespez, L., Lescure, S., Saulnier-Copard, S., Glais, A., Berger, J.F., Lavigne, F., et al., 2021. Discovery of a tsunami deposit from the Bronze Age Santorini eruption at Malia (Crete): impact, chronology, extension. Sci. Rep. 11 (1), 1–14.
Lin, G., Okubo, P.G., 2020. Seismic evidence for a shallow detachment beneath Kīlauea's south flank during the 2018 activity. Geophys. Res. Lett. 47 (15), e2020GL088003.
Lucchi, F., Peccerillo, A., Keller, J., Tranne, C.A., Rossi, P.L. (Eds.), 2013. The Aeolian Islands Volcanoes. Geological Society of London.
Micallef, A., Masson, D.G., Berndt, C., Stow, D.A., 2007. Morphology and mechanics of submarine spreading: a case study from the Storegga Slide. J. Geophys. Res., Earth Surf. 112 (F3).
Miramontes, E., Garziglia, S., Sultan, N., Jouet, G., Cattaneo, A., 2018. Morphological control of slope instability in contourites: a geotechnical approach. Landslides 15 (6), 1085–1095.
Mori, J., White, R., Harlow, D., Okubo, P., Power, J., Hoblitt, R., Laguerta, E., Lanuza, A., Baustista, C., 1994. Volcanic earthquakes following the 1991 climactic eruption of Mount Pinatubo: strong seismicity during a waning eruption. In: Fire and Mud: Eruptions and Lahars of Mount Pinatubo. Philippines, 1996, pp. 339–350.
Nomikou, P., Carey, S.N., Papanikolaou, D., Bell, K.L.C., Sakellariou, D., Alexandri, M., Bejelou, K., 2012. Submarine volcanoes of the Kolumbo volcanic zone NE of Santorini Caldera, Greece. J. Glob. Planet. Change 90, 135–151.
Nomikou, P., Parks, M.M., Papanikolaou, D., Pyle, D.M., Mather, T.A., Carey, S., et al., 2014. The emergence and growth of a submarine volcano: the Kameni islands, Santorini (Greece). GeoResJ 1, 8–18.
Nomikou, P., Druitt, T.H., Hübscher, C., Mather, T.A., Paulatto, M., Kalnins, L.M., et al., 2016. Post-eruptive flooding of Santorini caldera and implications for tsunami generation. Nat. Commun. 7 (1), 1–10.
Nomikou, P., Hübscher, C., Papanikolaou, D., Farangitakis, G.P., Ruhnau, M., Lampridou, D., 2018. Expanding extension, subsidence and lateral segmentation within the Santorini-Amorgos basins during Quaternary: implications for the 1956 Amorgos events, central-south Aegean Sea, Greece. Tectonophysics 722, 138–153.
Novikova, T., Papadopoulos, G.A., McCoy, F.W., 2011. Modelling of tsunami generated by the giant late Bronze Age eruption of Thera, South Aegean Sea, Greece. Geophys. J. Int. 186 (2), 665–680.
Paris, R., Smedile, A., Falvard, S., Devidal, J.L., Suchorski, K., 2022. A Minoan and a Neolithic tsunami recorded in coastal sediments of Ios Island, Aegean Sea, Greece. Mar. Geol. 106908.
Parks, M.M., Moore, J.D., Papanikolaou, X., Biggs, J., Mather, T.A., Pyle, D.M., et al., 2015. From quiescence to unrest: 20 years of satellite geodetic measurements at Santorini volcano, Greece. J. Geophys. Res., Solid Earth 120 (2), 1309–1328.
Poland, M.P., Peltier, A., Bonforte, A., Puglisi, G., 2017. The spectrum of persistent volcanic flank instability: a review and proposed framework based on Kīlauea, Piton de la Fournaise, and Etna. J. Volcanol. Geotherm. Res. 339, 63–80.
Pope, E.L., Jutzeler, M., Cartigny, M.J., Shreeve, J., Talling, P.J., Wright, I.C., Wysoczanski, R.J., 2018. Origin of spectacular fields of submarine sediment waves around volcanic islands. Earth Planet. Sci. Lett. 493, 12–24.
Preine, J., Karstens, J., Hübscher, C., Nomikou, P., Schmid, F., Crutchley, G.J., et al., 2022a. Spatio-temporal evolution of the Christiana-Santorini-Kolumbo volcanic field, Aegean Sea. Geology 50 (1), 96–100.
Preine, J., Karstens, J., Hübscher, C., Crutchley, G.J., Druitt, T.H., Schmid, F., Nomikou, P., 2022b. The Hidden Giant: how a rift pulse triggered a cascade of sector collapses and voluminous secondary mass-transport events in the early evolution of Santorini. Basin Res.
Preine, J., Hübscher, C., Karstens, J., Nomikou, P., 2022c. Volcano-tectonic evolution of the Christiana-Santorini-Kolumbo Rift Zone. Tectonics, e2022TC007524.
Puzrin, A.M., Gray, T.E., Hill, A.J., 2015. Significance of the actual nonlinear slope geometry for catastrophic failure in submarine landslides. Proc. R. Soc. A, Math. Phys. Eng. Sci. 471 (2175), 20140772.
Reiche, S., Hübscher, C., Brenner, S., Betzler, C., Hall, J.K., 2018. The role of internal waves in the late Quaternary evolution of the Israeli continental slope. Mar. Geol. 406, 177–192.
Satow, C., Gudmundsson, A., Gertisser, R., Ramsey, C.B., Bazargan, M., Pyle, D.M., et al., 2021. Eruptive activity of the Santorini Volcano controlled by sea-level rise and fall. Nat. Geosci. 14 (8), 586–592.
Seabrook, S., Mackay, K., Watson, S., Clare, M., Hunt, J., Yeo, I., et al., 2023. Pyroclastic density currents explain far-reaching and diverse seafloor impacts of the 2022 Hunga Tonga Hunga Ha'apai eruption. https://doi.org/10.21203/rs.3.rs-2395332/v1.
Siebert, L., Simkin, T., 2002. Volcanoes of the world: an illustrated catalog of Holocene volcanoes and their eruptions. In: Global Volcanism Program Digital Information Series, GVP-3. Smithsonian Institution. http://www.volcano.si.edu/world/.
Sigurdsson, H., Carey, S.N., Mandeville, C.W., 1991a. Krakatau. Natl. Geogr. Res. Explor. 7, 310–327.
Sigurdsson, H., Carey, S.N., Mandeville, C.W., Bronto, S., 1991b. Pyroclastic flows of the 1883 Krakatau eruption. EOS Trans. 72, 377–392.
Sigurdsson, H., Carey, S., Alexandri, M., Vougioukalakis, G., Croff, K.L., Roman, C., Sakellariou, D., Anagnostou, C., Rousakis, G., Ioakim, C., Gogou, A., Ballas, D., Misaridis, T., Nomikou, P., 2006. Marine investigations of Greece's Santorini volcanic field. Eos 87, 337–342.
Stix, J., Kobayashi, T., 2008. Magma dynamics and collapse mechanisms during four historic caldera-forming events. J. Geophys. Res., Solid Earth 113 (B9).
Symons, W.O., Sumner, E.J., Talling, P.J., Cartigny, M.J., Clare, M.A., 2016. Large-scale sediment waves and scours on the modern seafloor and their implications for the prevalence of supercritical flows. Mar. Geol. 371, 130–148.
Urlaub, M., Petersen, F., Gross, F., Bonforte, A., Puglisi, G., Guglielmino, F., et al., 2018. Gravitational collapse of Mount Etna's southeastern flank. Sci. Adv. 4 (10), eaat9700.
Van Wyk de Vries, B., Francis, P.W., 1997. Catastrophic collapse at stratovolcanoes induced by gradual volcano spreading. Nature 387 (6631), 387–390.

Walter, T.R., Haghshenas Haghighi, M., Schneider, F.M., Coppola, D., Motagh, M., Saul, J., et al., 2019. Complex hazard cascade culminating in the Anak Krakatau sector collapse. Nat. Commun. 10 (1), 1–11.
Watt, S.F.L., Talling, P.J., Vardy, M.E., Heller, V., Hühnerbach, V., Urlaub, M., et al., 2012. Combinations of volcanic-flank and seafloor-sediment failure offshore Montserrat, and their implications for tsunami generation. Earth Planet. Sci. Lett. 319, 228–240.
Wiemer, G., Kopf, A., 2017. On the role of volcanic ash deposits as preferential submarine slope failure planes. Landslides 14 (1), 223–232.
Yokoyama, I., 2001. The largest magnitudes of earthquakes associated with some historical eruptions and their volcanological significance. Ann. Geofis. 44, 1021–1029.